Implementation of Coupled-Trajectory Mixed Quantum Classical molecular dynamics for simulation of charge transport in organic and biological materials.

Matt Ellis

Supervisor: Jochen Blumberger

Second Supervisor: Graham Worth

MPhil Upgrade Report

Department of Physics and Astronomy

University College London

January 14, 2019

Abstract

Non-adiabatic processes play a vital role in many interesting processes such as photosynthesis, respiration and electronic charge transfers. In these systems the Born-Oppenheimer approximation cannot be applied and one must use computational simulations to model the physics. Many techniques have been proposed for this, all of which strike a compromise between accuracy and computation efficiency. To deal with realistic systems that have hundreds to thousands of molecules one must use mixed quantum-classical dynamics where the slow degrees of freedom (the nuclei) are treated classically and the fast ones treated with quantum mechanics. A range of techniques such as the Surface Hopping and Ehrenfest methods have been designed with this in mind. However, they tend to suffer from unphysical over-coherence issues. In this report, I present an implementation of a fragment-orbital based coupled-trajectory mixed quantum-classical algorithm (FOB-CTMQC), which is designed for simulating charge transport in systems of hundreds to thousands organic molecules. This method uses an in-house analytical overlap method (AOM) within the framework of coupled-trajectory mixed quantum-classical (CTMQC) molecular dynamics. CTMQC incorporates decoherence due to two new terms containing a quantity named the Quantum Momentum. I present several numerical tests of my implementation of the method. These include a demonstration of Rabi oscillation, energy conservation and a test of an essential equation used in the derivation of the CTMQC equations. I also discuss a problem in the norm conservation and an implementation of a smoothing function designed to overcome this.

Contents

Chapter 1

Introduction

1.1 Charge Transport Regimes in Organic Semiconductors

1.1.1 Organic Semiconductors

Conductive polymers were first discovered in 1977 by Shirakawa et al[1,2] for which they were awarded the Nobel prize in Chemistry. Recently these materials have become ubiquitous in many technologies, such as in organic solar cells[3], organic field-effect transistors (OFET)[4] and organic light-emitting diodes (OLED)[5]. While the other two technologies lag behind their inorganic counterparts, uptake of OLED screens is becoming increasingly popular -especially in the smartphone and television market due to their flexibility, better colour reprsentation and lower energy consumption than standard backlit LCD displays. In fact IHS markit's OLED market tracker predicts OLED to be the dominant technology in smartphone screens by 2020[6]. OLEDs have also found uses in lighting with their efficiency rivalling that of fluorescent tubes[7,8]. Although, industry has made large strides in fabricating and using these materials the exact nature of the charge transport is still poorly understood. Conventional hopping and band theories break down in the regime of partial delocalisation of the charge carriers and atomistic simulations are required for a realistic picture.

Typically charge carrier mobilities in 'good' organic semiconductors (OSCs) fall between 1-10 cm^2 V^{-1}s^{-1}[9]. This is just beyond the range of hopping model validity (~ 1 cm^2 V^{-1}s^{-1}) and below that of band theory (> 50 cm^2 V^{-1}s^{-1})[10]. In this intermediate regime the charge carriers are typically not completely delocalised at the valence band edges (band regime) or localised to a single site/molecule (hopping regime) but delocalised over a few molecules. Without any analytic approaches currently

being valid in this regime many computational approaches have been developed to investigate the underlying charge transport mechanisms[11].

1.2 Atomisitc Simulations of Nonadiabatic Processes

In simulating processes involving electronic transfers a key approximation used in conventional molecular dynamics (MD) breaks down. That is the Born-Oppenheimer or adiabatic approximation[12]. This approximation, relied upon for almost a century[13], hinges on the fact that nuclei are more massive than electrons and are approximately stationary with respect to electron movement[14]. This results in nuclear evolution that is governed by a single, adiabatic, potential energy surface. However, in many interesting processes, such as the proton coupled electron transfer in photosynthesis and respiration[15,16], non-radiative decay and photochemical processes, electronic transitions between adiabatic potential energy surfaces occur[17]. Simulating these processes requires non-adiabatic molecular dynamics (NAMD) techniques to be developed, to correctly capture dynamical properties.

There have been many techniques proposed for use in NAMD such as the quantum classical Louiville equation[18], multiple spawning[19] or nonadiabatic Bohmian dynamics[20]. However, two of the most popular are trajectory surface hopping[21] and mean-field approaches[22]. This is probably due to their relative simplicity to implement, efficiency for large systems and proven efficacy in a wide variety of situations[23]. In these approaches the general aim is to treat as much of the system as possible with (computionally cheaper) classical mechanics. While handling all necessary parts with quantum mechanics[24]. In Surface Hopping, Ehrenfest and Coupled-Trajectory Mixed Quantum-Classical molecular dynamics (CTMQC) one treats the nuclear subsystem classically and the electronic one quantum mechanically. The nuclei are propagated using a velocity verlet algorithm according to Newton's laws. The electrons are propagated using a fourth order Runge Kutta algorithm according to the time-dependent Schrödinger equation. This is normally expanded as a linear combination of adiabatic or diabatic states. The nuclei and electrons can also interact. Taking account of this interaction is where these different atomistic simulation techniques differ. Both trajectory surface hopping (SH) and Ehrenfest have significant downsides that the new algorithm CTMQC aims at overcoming with minimal computational overheads. In this project I will be developing an efficient implementation of CTMQC within the CP2K code.

1.2.1 Surface Hopping and Ehrenfest Dynamics

An important technique in the field of mixed quantum classical nonadiabatic molecular dynamics is Ehrenfest dynamics. Assuming we treat the nuclei classically the Ehrenfest equations can be rigorously derived from the electronic Schrödinger equation. This is done by assuming that the nuclei's motion is provided by a single population weighted average potential energy surface. This average is taken from the adiabatic potential energy surfaces (eigenvalues of the Hamiltonian) where weights are provided by the populations of each adiabatic state. This effective potential energy surface is shown in fig 1.1. In this way the electronic subsystem influences the propagation of the nuclei. The propagation of the forces and the electrons are controlled by equations (1.1) and (1.2).
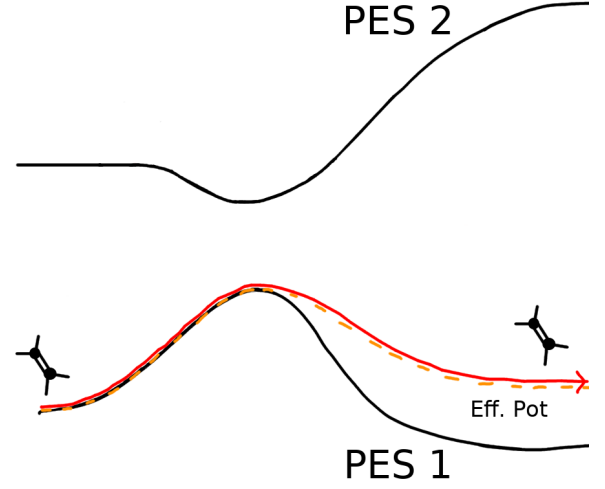

Figure 1.1: An example of a typical Ehrenfest simulation near an avoided crossing. The black lines represent the adiabatic potential energy surface due to the ground (PES 1) and excited (PES 2) state. The red line represents the population weighted average potential the nuclei travel on.

$$F_\nu^{Ehren} = \sum_i^{N_{st}} |C_i|^2 \nabla_\nu E_i + \sum_{i,j}^{N_{st}} C_i^* C_j (E_j - E_i) \mathbf{d}_{ij,\nu} \tag{1.1}$$

$$\hbar \vec{C}_m = C_m E_m - i\hbar \sum_n^{N_{st}} C_n d_{mn}^{ad} \tag{1.2}$$

In the above equations C_i is the adiabatic expansion coefficient for state i, E_m is the energy of adiabatic state m, $\mathbf{d}_{mn,\nu}^{ad}$ is the nonadiabatic coupling (in the adiabatic basis) between states m and n for atom ν. The d_{mn}^{ad} are the nonadiabtic coupling elements expressed in the adiabatic basis. Although the Ehrenfest method has been applied with success in many systems[25–27] it has a number of key shortcomings. Namely, its inability to capture the branching of the nuclear wavefunction as propagtion occurs on only a single potential energy surface and its poor account of the decoherence of the electronic and nuclear subsystem after an avoided crossing. Ehrenfest also violates detailed balance by populating all adiabatic states evenly[12,28]. In the limit of infinite states this results in infinite electronic temperature[29].

Possibly the most popular technique in NAMD is trajectory surface hopping. In trajectory surface hopping the shape of the potential energy surface is determined by a series of discrete stochastic hops between adiabatic potential energy surfaces[28]. See fig 1.2. The probability of these hops is determined by the non-adiabatic coupling between states. A swarm of trajectories are used and the probability a hop (non-adiabatic coupling) determines how many of these change state. The nuclear dynamics are dictated by the shape of the energy surface they are travelling on. This method can capture the branching of nuclear wavepacket unlike Ehrenfest. However, it still suffers from a number of issues. The original 'fewest switches surface hopping' proposed by John Tully suffered from bad overcoherence of the nuclear and electronic subsystems. That is the electronic and nu-

Figure 1.2: An example of a typical Surface Hopping simulation near an avoided crossing. The black lines represent the adiabatic potential energy surface due to the ground (PES 1) and excited (PES 2) state. The red line represents the discontinuous effectice potential the nuclei travel on.

clear motion was coupled long after the region of high non-adiabatic coupling (crossing region). The fact that the hops are instant leads to discontinuities and methods need to be implemented to fix these such as velocity re-scaling. Finally, perhaps the most important shortcoming is that this technique has not been derived from first principles and cannot be guaranteed to work generally. These problems have lead to a number of other techniques being developed. One of these, CTMQC, is the subject of this report.

1.2.2 Motivation for my Work

To overcome some of the challenges of the traditional Ehrenfest and Surface Hopping simulation techniques I plan to implement the newly proposed CTMQC technique[30]. This has been rigorously derived from the exact factorisation of the molecular wavefunction[31] and has been shown to work for toy model systems and a single molecule of Oxirane[30,32]. The equations appear to be the standard Ehrenfest equations with a correction provided by 2 new terms -the quantum momentum and a time-integrated adiabatic force. This correction allows a more theoretically rigorous handling of the

decoherence and nuclear wavepacket splitting seen in nonadiabatic systems.

This technique should not be much more expensive than either surface hopping or Ehrenfest and when paired with a FOB formalism (see section B) it should roughly scale as $\mathscr{O}(N_{mol}^3)$. Where N_{mol} is the number of molecules in the system. However, being a much newer technique, far less is known about it especially the new 'quantum momentum' and 'time-integrated adiabatic force' terms. This technique is also more difficult to code up than both trajectory surface hopping and Ehrenfest especially seeing as a trivial parallelisation strategy can no longer be used due to coupling between trajectories.

Chapter 2

CTMQC

2.1 Exact Factorisation

The exact factorisation of the molecular wavefunction[31] is the root of the derivation of the CTMQC equations so it is useful to study this. Exact factorisation involves separating the total molecular wavefunction into a nuclear component and electronic component. Where the electronic component is parametrically dependent on the nuclear coordinates, $\mathbf{R}$. This is shown below in eq (2.1) where χ is the nuclear wavefunction and Φ is the electronic one.

$$\Psi(\mathbf{R},\mathbf{r},t) = \Phi_{\mathbf{R}}(\mathbf{r},t)\chi(\mathbf{R},t) \tag{2.1}$$

In the above equation (and throughout this report) I will denote nuclear coordinates and electronic coordinates R and r respectively. The nuclear and electronic wavefunctions then obey separate, but coupled, time-dependent schrödinger equations for spatial and temporal evolution. This representation has proven to be useful in furthering understanding through exact solutions of small toy-model systems[30,33]. However, in this report I will be focussing on the semi-classical limit of these equations (CTMQC) and give some early results of a combination of this and the AOM method explained previously in section B. The equations for the evolution of the electronic and nuclear wavefunctions in the exact factorisation[31] are given below:

$$\hbar\frac{\delta}{\delta t}\Phi_{\mathbf{R}}(\mathbf{r},t) = \left(\hat{H}_{BO} + \hat{U}_{en}[\Phi_{\mathbf{R}},\chi] - \varepsilon(\mathbf{R},t)\right)\Phi_{\mathbf{R}}(\mathbf{r},t) \tag{2.2}$$

$$\hbar\frac{\delta}{\delta t}\chi(\mathbf{R},t) = \left(\sum_{\nu=1}^{N_n}\frac{[-\hbar\nabla_\nu + \mathbf{A}_\nu(\mathbf{R},t)]^2}{2M_\nu} + \varepsilon(\mathbf{R},t)\right)\chi(\mathbf{R},t) \tag{2.3}$$

Where $\hat{H}_{BO}$ is the Born-Oppenheimer Hamiltonian, that is $\hat{T}_e + \hat{W}_{ee} + \hat{W}_{nn} + \hat{V}_{en}$. Where $\hat{T}_e$ is the electronic kinetic energy operator, $\hat{W}_{ee/nn}$ is the electron-electron/nuclei-nuclei interaction and V_{en} is the electronic-nuclear potential.

The $\hat{U}_{en}$ is an electronic-nuclear coupling operator (ENCO). This is defined as

$$\hat{U}_{en}[\Phi_{\mathbf{R}}, \chi] = \sum_{v=1}^{N_{nuc}} \frac{1}{M_v} \left[\frac{[-\hbar\nabla_v - \mathbf{A}_v(\mathbf{R},t)]^2}{2} + \left(\frac{-\hbar\nabla_v\chi}{\chi} + \mathbf{A}_v(\mathbf{R},\mathbf{t}) \right)\left(-\hbar\nabla_v - \mathbf{A}_v(\mathbf{R},t) \right) \right]$$
(2.4)

Where the $\mathbf{A}_v$ is a time-dependent vector potential (TDVP), given by $\langle\Phi_{\mathbf{R}}(t)| -\hbar\nabla_v\Phi_{\mathbf{R}}\rangle_{\mathbf{r}}$ and M_v is the mass of nuclei v. Finally $\varepsilon(\mathbf{R},t)$ is a time-dependent scalar potential energy surface (TDPES), given by $\langle\Phi_{\mathbf{R}}(t)|\hat{H}_{BO} + \hat{U}_{en}^{coup} - \hbar\frac{\delta}{\delta t}|\Phi_{\mathbf{R}}(t)\rangle_{\mathbf{r}}$.

The effects of the TDPES, TDVP and the ENCO have been investigated in multiple works[32,34–37]. The TDPES and TDVP are both responsible for the evolution of the system[35]. The TDPES provides exact classical forces on the nuclei. In fact, an alternative independent-trajectory semi-classical scheme has been investigated using these exact forces[34]. This found the TDPES is responsible for the splitting of the nuclear wavepacket in regions of high non-adiabaticity by taking the shape of a step function between the 2 adiabatic potentials. This is demonstrated

Figure 2.1: A demonstration of how the TDPES can cause the splitting of the nuclear wavepacket in non-adiabatic regions. The red line represents the TDPES and the blue is the nuclear density. Adapted from[34]

in figure 2.1. Finally the electronic-nuclear coupling operator (ENCO) is responsible for other non-adiabatic effects in the system such as electronic nonadiabtic transitions and decoherence[35].
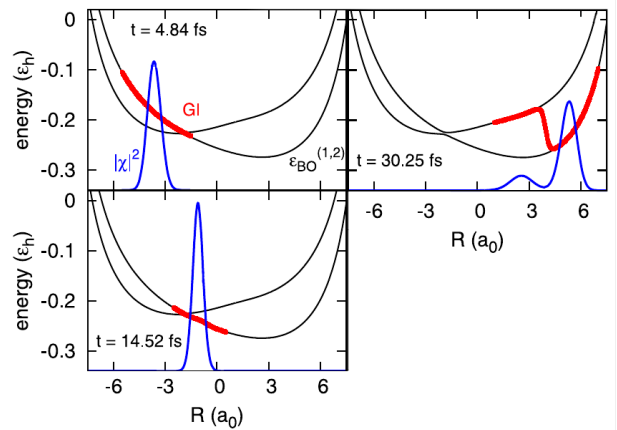
2.2 Approximations leading to CTMQC

Starting from the exact factorisation equations 6 approximations have been made to derive the CT-MQC equations. These are discussed in detail in Ref.[30]. In the interest of completeness I have summarised them below.

2.2.1 Classical Nuclei

Techniques that include nuclear quantum effects (NQEs); such as multiple spawning[19], ring-polymer surface hopping[38] and nonadiabatic Bohmian dynamics[39,40] although extremely accurate, cannot be applied to hundreds or thousands of molecules. This is due to their high computational cost. Further, in many systems of interest NQEs are negligible, especially at room temperature. For this reason the classical limit of the nuclear Schrödinger equation (2.3) is taken when deriving the CTMQC equations.

2.2.2 Neglect the ENCO in the TDPES

The electron-nuclei coupling operator is omitted in the expression for the time-dependent potential energy surface. This is justified as the first term ($[-\hbar\nabla_\nu - \mathbf{A}_\nu(\mathbf{R},t)]^2$) contains a second order derivative which is expensive to calculate and has a neglible effect compared to the second term in the ENCO[41]. However, the rest of the ENCO is equal to zero when averaged over $\Phi_\mathbf{R}(\mathbf{r},t)$ so it does not contribute to the TDPES.

2.2.3 Derivative of the Adiabatic Coefficients

The derivative of the adiabatic coefficients appears in the electronic evolution equations. However, we can re-write the derivative of the adiabatic coefficients in terms of their modulus and phase:

$$\nabla_\nu C_l^{(I)}(t) = \left[\underbrace{\frac{\nabla_\nu |C_l^{(I)}(t)|}{|C_l^{(I)}(t)|}}_{\text{(Term 1)}} + \underbrace{\frac{i}{\hbar}\nabla_\nu \gamma_l^{(I)}(t)}_{\text{(Term 2)}} \right] C_l^{(I)}(t) \tag{2.5}$$

It has been found that the first term is negligible compared to the second[32,34,36] so it doesn't need to be calculated and we can remove it. It was also assumed that the NACVs are localised in space

meaning that, after some algebra, the spatial derivative of the adiabatic coefficient can be written as:

$$\nabla_\nu C_l^{(I)}(t) = \frac{i}{\hbar} \nabla_\nu \gamma_l^{(I)}(t) C_l^{(I)}(t) = -\frac{i}{\hbar} \int^t dt' \nabla_\nu \varepsilon_l^{(I)} C_l^{(I)}(t) = -\frac{i}{\hbar} \mathbf{f}_l^{(I)} C_l^{(I)}(t) \tag{2.6}$$

Where $\varepsilon_l^{(I)}$ is the energy of the lth adiabatic potential energy surface for trajectory I, $C_l^{(I)}$ is the adiabatic expansion coefficient for state l and trajectory I. The $\mathbf{f}_l^{(I)}$ is the time-integrated adiabatic force.

2.2.4 Gaussian Nuclear Wavepackets

In order to calculate the quantum momentum -the new term in CTMQC. Knowledge of the nuclear distribution is needed. To this end the nuclear wavepacket is assumed to take the shape of a Gaussian. This is centred on the atomic coordinate with a width σ. In this work I have used a constant width throughout, with plans to implement dynamic Gaussian width calculations later. However, the nuclei are still propagated classically, the width parameter is only used in the calculation of the quantum momentum.

2.2.5 Seperating the Effects of Decoherence and NACVs

So as to not introduce any population transfer (due to the quantum momentum) when the NACV is zero a fifth approximation has been introduced. Namely the quantum momentum depends on pairs of states -l,k. This enables the separation of the 'competing' effects of the NACV and the Quantum Momentum.

2.3 The CTMQC equations

2.3.1 Adiabatic Basis

The equations for the propagation of the classical nuclei and the expansion coefficients in the CTMQC framework in the adiabatic basis are given below:

$$\dot{\mathbf{P}}_\nu^{(I)} = -\overbrace{\sum_k |C_k^{(I)}|^2 \nabla_\nu \varepsilon_k^{(I)} - \sum_{k,l} C_l^{(I)} C_k^{*(I)} \left(\varepsilon_k^{(I)} - \varepsilon_l^{(I)} \right)}^{\text{Ehrenfest}}$$
$$\underbrace{-\sum_{l,k} |C_l^{(I)}|^2 \left(\sum_{v'=1}^{N_n} \frac{2}{\hbar M_{v'}} \mathscr{Q}_{lk,\nu}^{(I)} \cdot \mathbf{f}_{l,\nu}^{(I)} \right) \left[|C_k^{(I)}|^2 \mathbf{f}_{k,\nu}^{(I)} - \mathbf{f}_{l,\nu}^{(I)} \right]}_{\text{Quantum Momentum}} \tag{2.7}$$

$$\dot{C}_l^{(I)} = \overbrace{-\frac{i}{\hbar}\varepsilon_l^{(I)}C_l - \sum_k C_k^{(I)}d_{lk}^{ad\ (I)}}^{\text{Ehrenfest}}$$

$$\underbrace{-\sum_{\nu=1}^{N_n}\sum_k \frac{\mathcal{Q}_{lk,\nu}^{(I)}}{\hbar M_\nu}\cdot\left[\mathbf{f}_{k,\nu}^{(I)} - \mathbf{f}_{l,\nu}^{(I)}\right]|C_k^{(I)}|^2 C_l^{(I)}}_{\text{Quantum Momentum}}$$

(2.8)

Where the ε_k term is the potential energy on the kth potential energy surface. C_l is the adiabatic expansion coefficient corresponding to the lth state. The sum over k and l indicates a sum over all states, the (I) superscript is a replica index and the ν is an atom index. M_ν is the nuclear mass and $d_{lk}^{(I)}$ represents the non-adiabatic coupling element (in the adiabatic basis) between adiabatic states l and k, $\langle\psi_l|\frac{d}{dt}\psi_k\rangle$. The 2 new terms in this scheme not seen in other one are the $\mathcal{Q}_{lk,\nu}^{(I)}$ and the $\mathbf{f}_{k,\nu}^{(I)}$. These are the quantum momentum and the history dependent adiabatic force. The history dependent force in defined in equation (2.6) this keeps a record of the previous forces in the system. The quantum momentum term couples the trajectories together (making this a coupled-trajectory scheme). Together the history dependent force and quantum momentum are responsible for the decoherence in the 'Quantum Momentum' parts of the above equations[33]. Notably, although these equations have been derived from the exact factorisation equations separately from Ehrenfest they do contain exactly the Ehrenfest equations within them (marked 'Ehrenfest'). This scheme can therefore be seen as an Ehrenfest scheme with a correction that captures branching of the nuclear wavefunction and decoherence within it.

We can also see in equation (2.8) if we are in a pure adiabatic state i.e. all population on a single adiabatic state, there is no contribution from the quantum momentum part of the equations. In this scenario the evolution equations become simply Ehrenfest equations. For example, if we only have 1 state in the system with non-zero adiabatic population then the term $|C_k^{(I)}|^2 C_l$ is only non-zero when $l = k$. However, when $l = k$, the term $\left[\mathbf{f}_{k,\nu}^{(I)} - \mathbf{f}_{l,\nu}^{(I)}\right]$ is zero as $\mathbf{f}_{k,\nu}^{(I)} = \mathbf{f}_{l,\nu}^{(I)}$. Therefore, the quantum momentum term can be seen to only kick in when there is a mixing of adiabatic states. In the adiabatic formulation of these equations it is the adiabatic NACV $\mathbf{d}_{lk,\nu}^{ad,(I)}$ that is responsible for the initial mixing of the populations from pure adiabatic states.

2.3.2 Diabatic Basis

The equations above (2.7) & (2.8) are both in the adiabatic basis. However, to make use of the FOB-formalism detailed in appendix B already implemented in the CP2K software package[42] these need to be transformed to the orthogonal diabatic basis, ϕ. After applying the transformation matrix $\mathbb{U}$ and some algebra the equations in the diabatic basis can be written as:

$$
F_v^{(I)}(t) = \overbrace{-\sum_{l,k} u_l^{(I)*} u_k^{(I)} \nabla_v H_{lk}^{(I)} - \sum_{l,k,a} d_{la}^{(I)} H_{ak}^{(I)} - d_{ak}^{(I)} H_{la}^{(I)}}^{\text{Ehrenfest}}
$$
$$
\underbrace{-2\sum_l |C_l^{(I)}|^2 \sum_n \left(\sum_{v'}^N \frac{\mathscr{Q}_{ln,v'}^{(I)}(t)}{\hbar M_{v'}} \cdot \mathbf{f}_{l,v'}^{(I)} \right) \left[|C_n^{(I)}|^2 \mathbf{f}_{n,v}^{(I)} - \mathbf{f}_{l,v}^{(I)} \right]}_{\text{Quantum Momentum}}
\tag{2.9}
$$

$$
\dot{u}_k^{(I)} = \overbrace{-\frac{i}{\hbar} \sum_l u_l^{(I)} \left(H_{kl}^{(I)} + \hbar d_{kl}^{(I)} \right)}^{\text{Ehrenfest}}
\tag{2.10}
$$

$$
\underbrace{+ \sum_s U_{ks} \sum_{v=1}^{N_n} \sum_n \frac{\mathscr{Q}_{sn,v}^{(I)}}{\hbar M_v} \cdot \left[\mathbf{f}_{n,v}^{(I)} - \mathbf{f}_{s,v}^{(I)} \right] |C_n^{(I)}|^2 \sum_l U_{sl}^* u_l^{(I)}}_{\text{Quantum Momentum}}
\tag{2.11}
$$

Where $u_l^{(I)}$ represents the diabatic expansion coefficient for (orthogonal) diabatic state l on trajectory I. $H_{kl}^{(I)} = \langle \phi_k^{(I)} | H^{(I)} | \phi_l^{(I)} \rangle$ is the diabatic Hamiltonian. $d_{kl} = \langle \phi_k^{(I)} | \dot{\phi}_l^{(I)} \rangle$ is the non-adiabatic coupling element (NACE) expressed in the quassi diabatic basis. This is usually very small but not zero due to the basis not being a true diabatic one. $U_{ks} = \langle \phi_k | \psi_s \rangle$ is the adiabatic-diabatic transformation matrix. The other terms have been previously defined in the adiabatic equations (see section 2.3.1).

The 2 expressions can again be decomposed into a quantum momentum part and an Ehrenfest part. In the force expression (2.9) the Ehrenfest part comprises 2 terms. In tests I have found the first term contributes significantly more to the overall force than the second 'commutator' term. This means that the second term, can be neglected in most situations. The quantum momentum term in the force expression is expressed in the adiabatic basis. This is because it is basis independent and numerically transforming it with transformation matrices would result in unnecessary computation. The quantum momentum part of the electronic equation (2.11) is largely unchanged compared to

the adiabatic one (2.8) and an on-the-fly transformation from adiabatic to diabatic representations is required during propagation.

The diabatic hamiltonian, as opposed to the adiabatic one, now contains non-zero off-diagonal elements. This is the primary term responsible for population transfer when in pure adiabatic states. The diabatic NACE has a much smaller effect as it is comparatively very small.

2.4 Calculating the Quantum Momentum

The technique for calculating the quantum momentum term is outlined in detail in the SI of[43]. The original equations given in[30] present a quantum momentum term without state indices (l,k). This, due to approximations made in the derivation of CTMQC, results in population transfer even when the non-adiabatic couplings between states are zero. Therefore Agostini et al has enforced this with the pair-wise state dependence of the quantum momentum.

The quantum momentum is defined as:

$$\mathscr{Q}_v^{(I)} = \frac{-\hbar \nabla_v |\chi^{(I)}|}{|\chi^{(I)}|} \frac{-\hbar \nabla_v |\chi^{(I)}|^2}{2|\chi^{(I)}|^2} \tag{2.12}$$

In order to reconstruct the nuclear density Gaussian distributions can be used. This results in a linear expression for the quantum momentum. The full details of the derivation are given in the supplementary information of[43]. The resulting linear expression for the quantum momentum is given below:

$$\mathscr{Q}_{lk,v}^{(I)} = \alpha_v^{(I)} \mathbf{R}_v^{(I)} - \mathbf{R}_{lk,v} \tag{2.13}$$

Where $\mathbf{R}_v^{(I)}$ are the nuclear coordinates on trajectory I on atom v. The $\alpha_v^{(I)}$ term is a weighted average over trajectories of the product of the gaussian's assigned to each atomic coordinate, i.e:

$$\alpha_v^{(I)} = \sum_J^{N_{tr}} \frac{\hbar \prod_{v'} g_{\sigma_{v'}^{(J)}(t)} \left(\mathbf{R}_{v'}^{(I)}(t) - \mathbf{R}_{v'}^{(J)}(t) \right)}{2\sigma_v^{(J)}(t)^2 \sum_K^{N_{tr}} \prod_{v'} g_{\sigma_{v'}^{(K)}(t)} \left(\mathbf{R}_{v'}^{(I)}(t) - \mathbf{R}_{v'}^{(K)}(t) \right)} \tag{2.14}$$

Where $\sigma_{v'}^{(J)}(t)$ is a width parameter for the width of the gaussian centered at atomic coordinates. Along with the $\mathbf{R}_{lk,v}$ term the $\alpha_v^{(I)}$ performs the job of coupling the trajectories together. The $\mathbf{R}_{lk,v}$ term also given in the SI of[43] is defined for each cartesian dimension as:

$$R_{lk,v} = \sum_I^{N_{tr}} R_v^{(I)}(t) \alpha_v^{(I)}(t) \frac{|C_k^{(I)}(t)|^2 |C_l^{(I)}(t)|^2 \left(f_{k,v}^{(I)}(t) - f_{l,v}^{(I)}(t)\right)}{\sum_J |C_k^{(J)}(t)|^2 |C_l^{(J)}(t)|^2 \left(f_{k,v}^{(J)}(t) - f_{l,v}^{(J)}(t)\right)} \tag{2.15}$$

Where the bold notation for vectors has been replaced by normal font indicating that this applies to each cartesian dimension independently. Further, in this expression $R_{lk,v}$ is anti-symmetric, $R_{lk} = R_{kl}$ meaning that $Q_{lk} = Q_{kl}$. At first sight the R_{lk} term seems to be another weighted average. However, this isn't quite the case as the denominator can have negative terms. This causes equation (2.15) to be very sensitive to errors in the calculation of the denominator of this fraction. Any inaccuracies can lead to the denominator approaching zero faster than the numerator causing large spikes in the quantum momentum term.

2.5 Testing my Implementation

I have implemented a serial version of this algorithm in the CP2K software package[42]. As well as many numerical tests on individual terms in the equations, I have implemented some physical tests too. In this section I will outline some of the key tests I have performed on both the Ehrenfest part of the equations and the full CTMQC equations.

A typical system for the following tests consists of a dimer of ethylene-like molecules. These are called ethylene-like molecules as their parameters (such as electronic coupling and reorganisation energy) are varied to investigate different regimes. The Hamiltonian is constructed using an analytical overlap method (dicussed in detail in appendix B and ref[44]). The diagonal elements of this Hamiltonian come from a classical forcefield and the off-diagonal one are assumed to be proportional to the overlap between orbitals on the molecules. This technique circumvents the need for using expensive density functional theory methods to calculate the electronic structure and has been shown to give results for pi-conjugated systems within chemical accuracy[44].

2.5.1 Rabi Oscillation

Rabi Oscillation can be shown to occur in systems that have fixed nuclear geometries (see section A.2). During Rabi oscillation the electronic dynamics are given by an analytic formula. This can be solved in Python and used to test the implementation of the electonic propagation, decoupled from nuclear dynamics. In this test Ehrenfest was used to propagate the system, which consisted of a trimer of an Ethylene-like molecule with 10 replicas. Each of the replicas were initialised with different positions. The electronic propagation of Ehrenfest is the same as that of trajectory surface hopping so I have adapted a previously implemented subroutine from the FOB-SH method[44] to work for many replicas. The results are shown in figure 2.2.
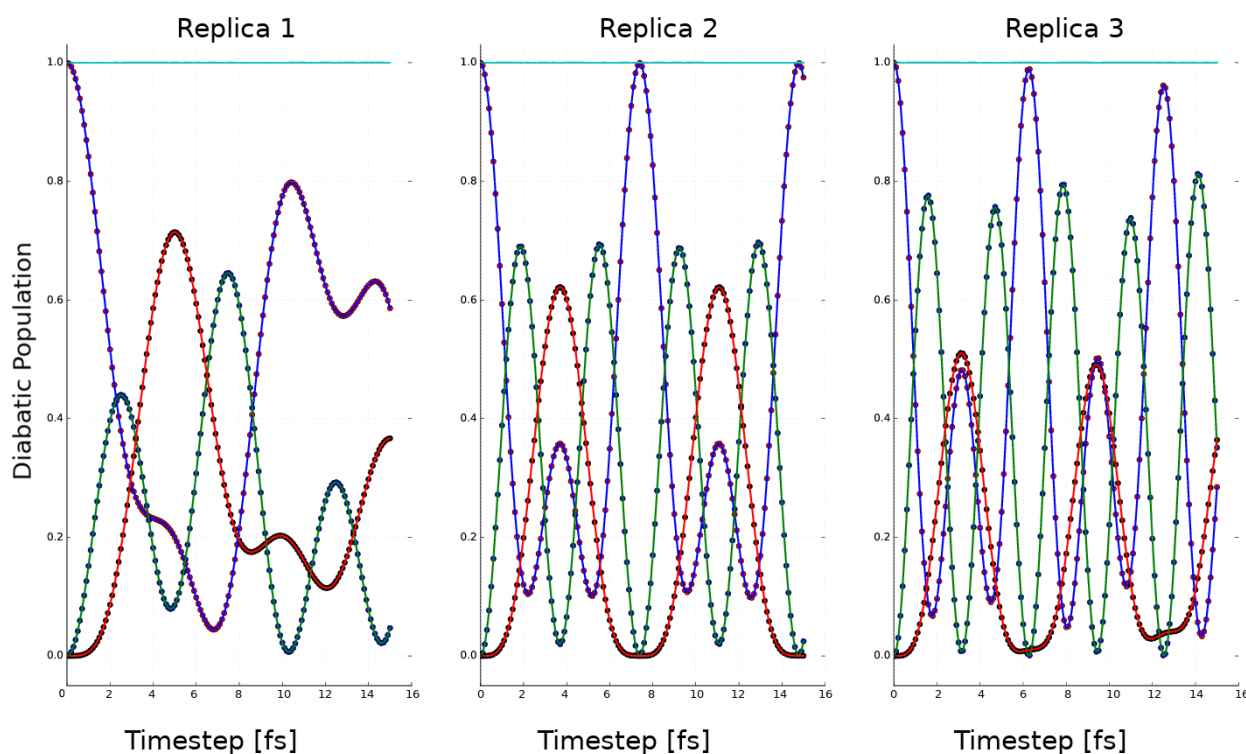

Figure 2.2: Rabi oscillation for a trimer of Ethylene, results shown for 3 replicas. Solid lines indicate the output of the CP2K propagation and dots indicate the result of the analytic Rabi formula. Different colors indicate different states. The cyan line shows the sum of the diabatic populations i.e. the norm.

We can see in figure 2.2 CP2K gives the same output as the analytic result. This means for Ehrenfest the electronic propagation is working as expected. Molecules in replica 1 were initialised further apart than those of replica 2 and replica 3, with replica 3 having the closest molecules. We can see that the frequency of oscillation of charge between molecules that are further apart is slower. Something we

would expect to see in a realistic system. Further the new implementation of multiple replicas can be seen to work with all replicas give correct results.

2.5.2 Energy Conservation

The Ehrenfest equations can be shown to conserve the potential energy + total kinetic energy[45]. The potential energy is given by the effective potential (i.e. $\sum_l |C_l^{(I)}|^2 \varepsilon_l$) and the total kinetic energy is given as a sum of the kinetic energy over all atoms. In this test the commutator term was neglected from equation (2.9). 8 simulations were performed. These used the same initial conditions but varied a random number generator seed, which is used in the calculation of the NACVs. In each simulation 100 replicas were used over various couplings and averaged to get the average energy drift per replica. The error bar was obtained from the average energy drifts of the 8 simulations.
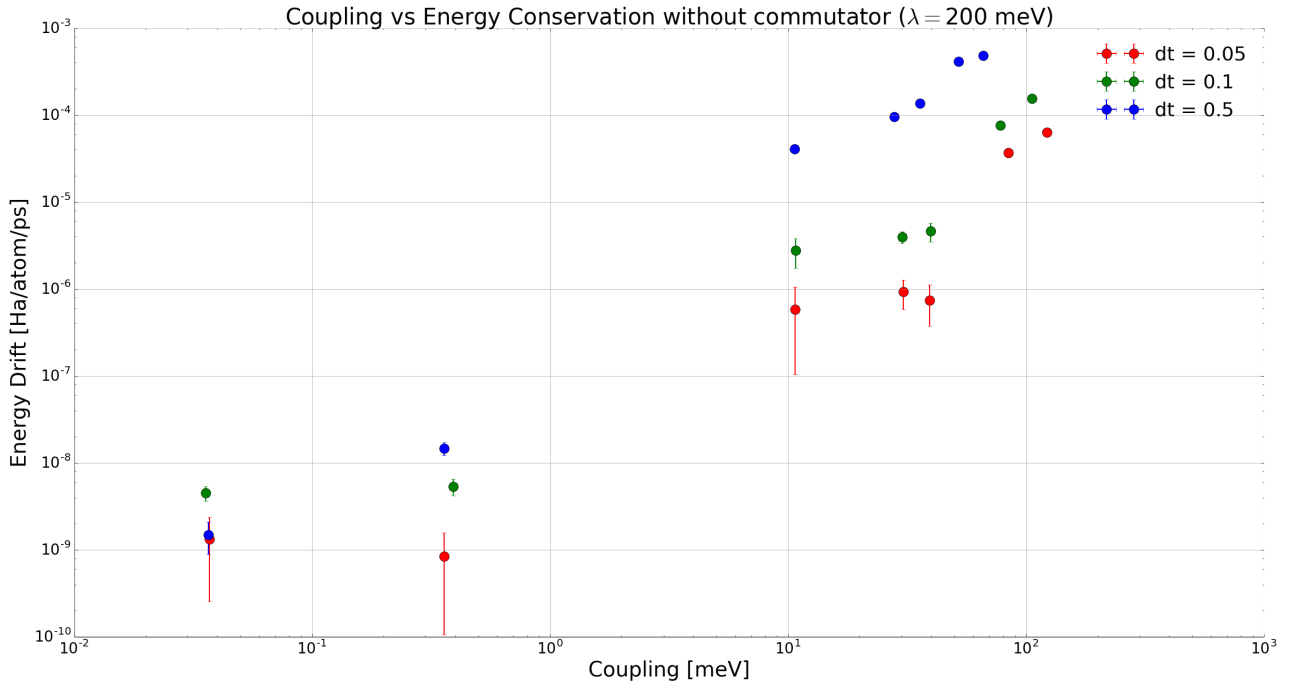
Figure 2.3: Energy drift in Ehrenfest for various couplings. Each color represents a different nuclear time-step used in fs.

We can see that the energy is conserved very well for low couplings and starts to increase for higher ones. The exact reason for this is not known. It may be due to the fact the the effective potential energy surface is a population weighted average. If the energies are closer together around the crossing region (as in lower coupling systems) then this average becomes a better representation of the true

potential. When the states are further apart the average becomes more of an approximation. From this graph a time-step of 0.1fs was chosen as a compromise between accuracy and computational cost.

2.5.3 Norm Conservation

The norm of the coefficients should be conserved when propagating the equations. To not do so would mean that the total number of charge carriers is changing, i.e. electrons/holes being destroyed or created. Both the CTMQC and Ehrenfest electronic equations can be shown to conserve the norm (see appendix A.1). When propagating Ehrenfest dynamics this is very well conserved, with norm drifts (using a nuclear time-step of 0.1fs) on the order 10^{-10} ps^{-1}. However, in CTMQC the story is slightly different.

The quantum momentum appears in both the nuclear force equation and the electronic equation. However, its current formulation using Gaussian distributions to model the nuclear density results in equation (2.13). That is $\mathcal{Q}_{lk,v}^{(I)} = \alpha_v^{(I)} \mathbf{R}_v^{(I)} - \mathbf{R}_{lk,v}^{(I)}$. Where the $\mathbf{R}_{lk,v}^{(I)}$ term is calculated via equation (2.15). This is given again below in a condensed form:

$$\mathbf{R}_{lk,v} = \sum_{I}^{N_{tr}} R_v^{(I)}(t)\alpha_v^{(I)}(t)\frac{\mathbf{Y}_{lk,v}^{(I)}(t)}{\sum_{J}\mathbf{Y}_{lk,v}^{(I)}(t)}$$

Where $\mathbf{Y}_{lk,v}^{(I)} = |C_k^{(J)}(t)|^2|C_l^{(J)}(t)|^2\left(\mathbf{f}_{k,v}^{(J)}(t) - \mathbf{f}_{l,v}^{(J)}(t)\right)$.

Due to the fact that $\mathbf{Y}_{lk,v}^{(I)}$ can be both negative and positive, the denominator of the $\mathbf{R}_{lk,v}$ equation can approach zero. Large spikes in the $\mathbf{R}_{lk,v}$ will be seen if this term approaches zero faster than the numerator. This can cause large spikes in the $\mathcal{Q}_{lk,v}^{(I)}$ resulting in an amplification of any inaccuracies in the $\mathbf{Y}_{lk,v}^{(I)}$ term. In my simulations this has resulted in a very bad conservation of the norm. A demonstration of this can be seen below in figure 2.4. This shows that the denominator of the $\mathbf{R}_{lk,v}^{(I)}$ term approaching zero can cause spikes in the quantum momentum. These spike in the quantum momentum can affect the nuclear and electronic propagation. One way this manifests itself is in bad norm conservation. This is shown in figure 2.5 below, where the large spike in the quantum momentum appears as a discontinuity in the norm.
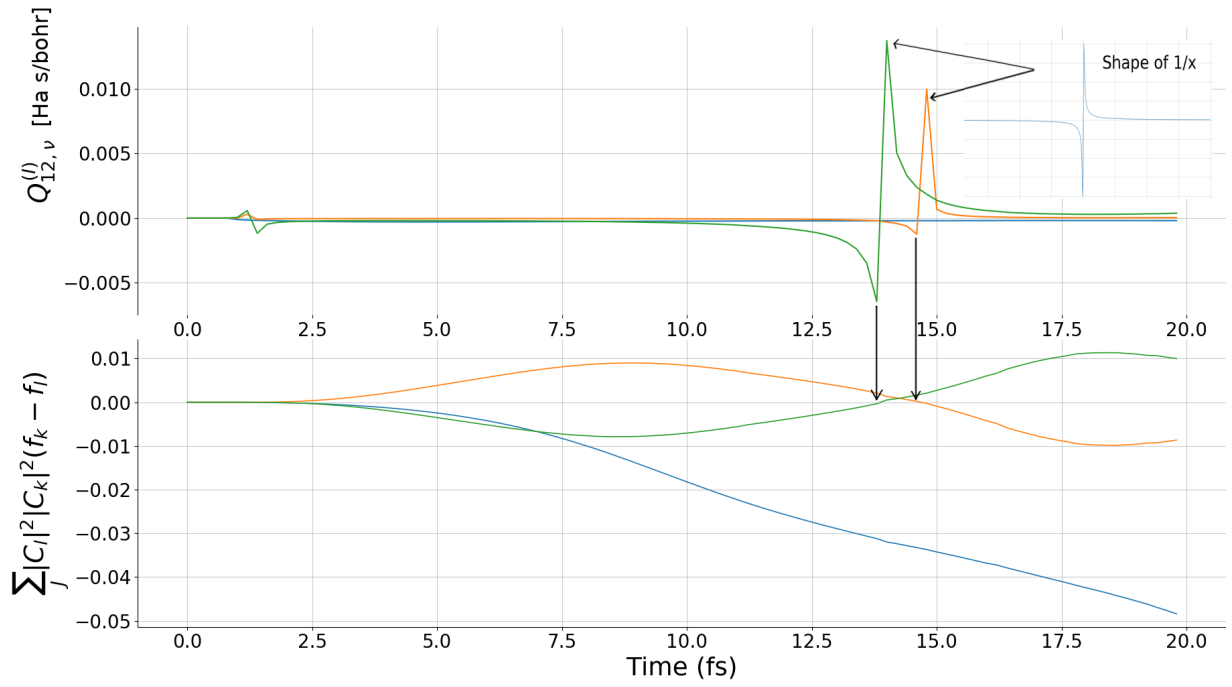
Figure 2.4: A time-series plot of the denominator in the $\mathbf{R}_{lk,\nu}$ equation (bottom graph) and the quantum momentum term between states 1 & 2 on atom 1 for replica 1 (top graph). Each colour represents a different cartesian component.
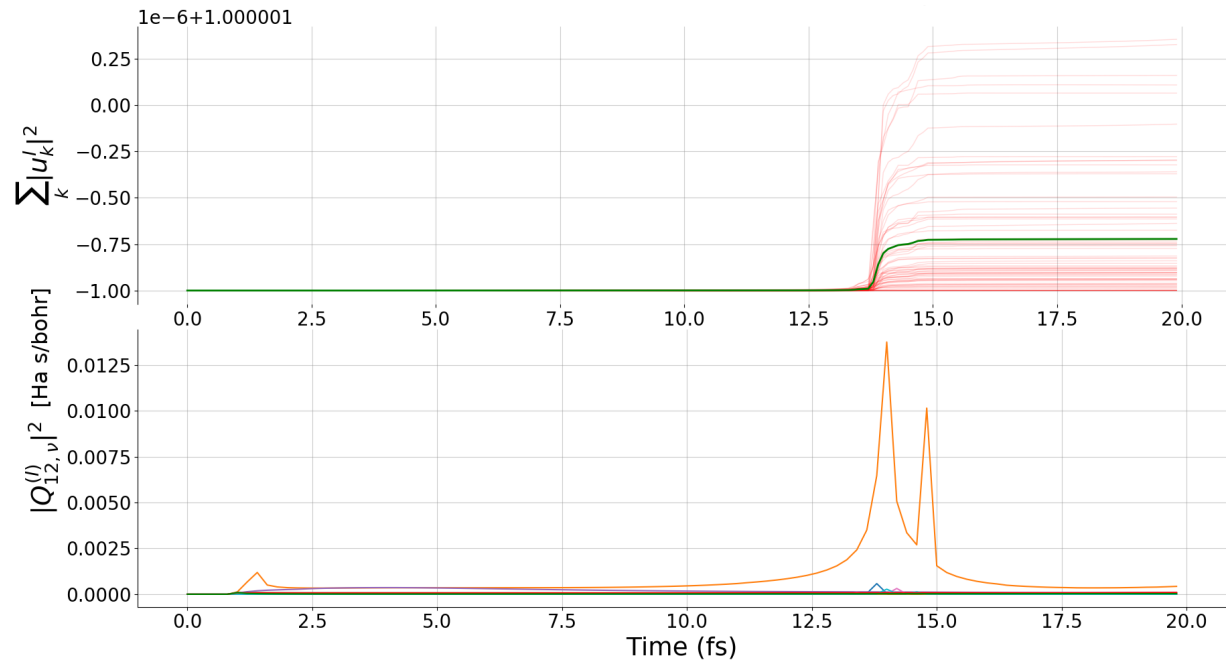

Figure 2.5: A time-series plot of the squared magnitude of the quantum momentum between states 1 & 2 on atom 1 for replica 1 (bottom graph) and the norm of the diabatic expansion coefficients (top graph).

In an attempt to counter this problem a smoothing function has been implemented in the calculation of the $R_{lk,v}$ term. This takes the shape of a $\tanh(\frac{a}{x})^2$ function, that is:

$$\mathbf{R}_{lk,v} = \sum_I^{N_{tr}} R_v^{(I)}(t) \alpha_v^{(I)}(t) \frac{\mathbf{Y}_{lk,v}^{(I)}(t)}{\sum_J \mathbf{Y}_{lk,v}^{(I)}(t)} \underbrace{\tanh\left(\frac{\sum_J \mathbf{Y}_{lk,v}^{(I)}(t)}{W}\right)^2}_{\text{smoothing parameter}} \tag{2.16}$$

By altering the 'width' parameter, W, one can set the level of smoothing of the spikes in the quantum momentum term. As this width approaches 0, or as the $\mathbf{Y}_{lk,v}^{(I)}(t)$ term approaches ∞ the standard expression for the $\mathbf{R}_{lk,v}$ term is retrieved. When the value inside the tanh expression is larger than ~ 3 the smoothing term has a very small effect. This means this parameter will only alter the calculation of the quantum momentum if the $\mathbf{Y}_{lk,v}^{(I)}(t)$ term (the denominator of $\mathbf{R}_{lk,v}$) is smaller than some width, W, divided by 3. The results of the implementation of this is shown below in figure 2.6.
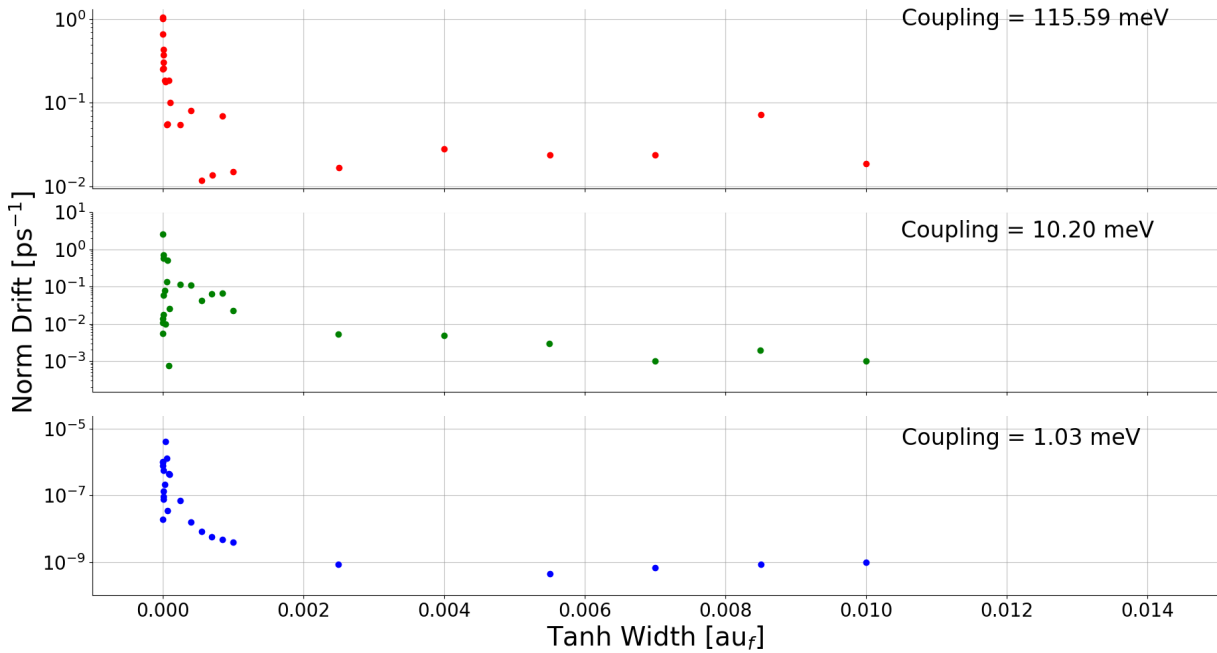
Figure 2.6: A figure showing the change in the norm conservation with a varying tanh width for 3 different electronic couplings, 100 meV (top), 10 meV (middle) 1 meV (bottom).

An improvement spanning several orders of magnitude can be seen in figure 2.6 for all couplings. However, there is still room for improvement, especially in the higher 2 couplings. Renormalisation at each time-step is necessary to correct small average errors, a more elaborate scheme with a dynamic

smoothing width may be required for larger more complex systems.

2.5.4 Time-Derivative of the Sum Over Trajectories of Adiabatic Populations

In the supplementary information of Min, 17[43] a further condition was imposed when deriving the equation for the Quantum Momentum (equation S26). This is given below:

$$\sum_{I}^{N_{rep}} \frac{d|C_{qm,l}^{(I)}|^2}{dt} = \sum_{I}^{N_{rep}} \sum_{\nu}^{N_n} 2 \frac{\mathscr{Q}_{lk,\nu}^{(I)}}{\hbar M_\nu} \cdot \left(\mathbf{f}_{k,\nu}^{(I)} - \mathbf{f}_{l,\nu}^{(I)}\right) |C_l^{(I)}|^2 |C_k^{(I)}|^2 = 0 \qquad \forall l,k \qquad (2.17)$$

This equation can be used to monitor the dynamics and test the Quantum Momentum calculation. Figure 2.7 below shows the result of this for an arbitrary coupling (10meV) in a dimer of an Ethylene like molecule.

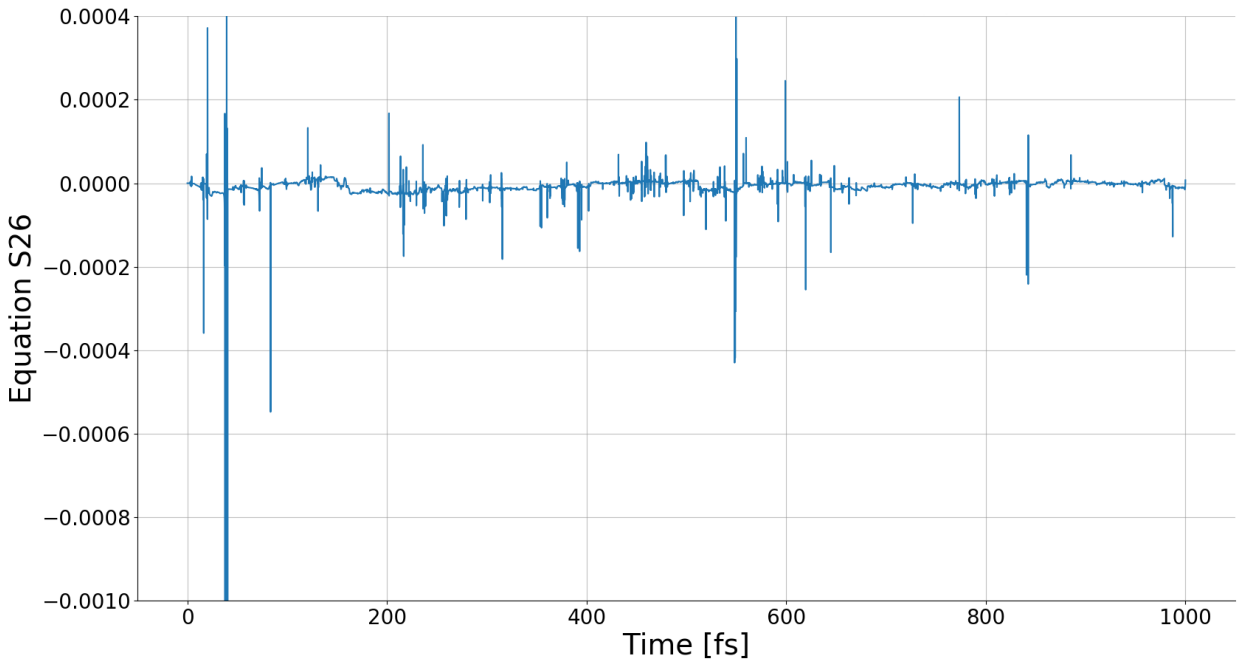**Figure 2.7:** Equation S26 from[43]. A coupling of 10meV was used and a tanh smoothing width was 0.0001 au$_f$.

We can see that the equation is fulfilled to within $\sim 10^{-5}$ with some fairly large spikes. These spikes are caused by a spike in the quantum momentum due to denominator in the $\mathbf{R}_{lk,\nu}$ equation (2.15) approaching zero. This assures me that the quantum momentum is implemented correctly.

Chapter 3

General Conclusions

There are many real world applications of organic semiconductors[46–48] and accurate models of charge transport are important to facilitate new materials discovery and characterisation. However, due to mobilities falling within an intermediate region where neither band theories nor hopping theories are applicable non-adiabatic atomistic simulations must be used[11]. Among the litany of techniques proposed there are no single silver bullets. As always, the user must make the compromise between accurate dynamics and computational cost. Two of the most popular mixed-quantum classical techniques are trajectory surface hopping (TSH) and Ehrenfest. However, these both suffer from well known problems such as over-coherent nuclear-electronic dynamics no branching of the nuclear wavefunction in Ehrenfest and lack of a first-principles grounding in TSH.

To overcome these challenges a new technique, coupled-trajectory mixed-quantum classical molecular dynamics (CTMQC), has been proposed[35] to more rigorously account for decoherence, branching of the nuclear wavefunction and to provide a technique based in first principles physics. This technique, derived from the exact factorisation of the molecular wavefunction[31], appears as a 'corrected' Ehrenfest scheme where the correction comes from 2 new terms -an adiabatic time-integrated force and a quantum momentum.

In this report I have outlined an implementation of CTMQC paired with a fragment-orbital based (FOB) technique to produce an efficient FOB-CTMQC propagator capable of simulating hundreds of organic molecules. The FOB method is based on the assumption that the electronic couplings (off-diagonal Hamiltonian elements) are proportional to the overlap between singly occupied molec-

ular orbitals (SOMOs). This approximation has been validated in many organic semiconductors and provides a significant speed-up when compared to using density functional theory.

The implementation process is still under progress. However, initial results are promising. Some key tests have been discussed including Rabi oscillation, energy conservation, norm conservation and the fulfilment of a fundamental equation (2.17). The tests have been mostly positive. However, due a denominator in the equation for calculating the quantum momentum approaching zero -causing the quantum momentum to spike. The norm was not well conserved and a smoothing $\tanh^2$ function was used to fix this.

To build on this work I would now like to apply FOB-CTMQC to more realistic systems and to eventually compare with experimental results. However, a number of tasks must be completed before this is possible. These include implementing a sensible algorithm for calculating the nuclear width parameter, σ_v^I, used in the calculation of the quantum momentum. This determines the width of the gaussians that combine to give the quantum momentum. I am currently using a frozen width of $\sqrt{2}$ bohr. The norm conservation and the spikes in the quantum momentum should be monitored also, if these get worse an improved smoothing algorithm will have to be implemented. Over the next year I would like to also test whether detailed balance is reached in CTMQC as well as comparing CTMQC with our in-house FOB-SH algorithm as well as with more accurate methods. CTMQC should be more accurate than the surface hopping (FOB-SH) algorithm and handle decoherence in a better way. For smaller systems CTMQC can be benchmarked against more accurate results such as the multi-configuration time-dependent Hartree method discussed here[49]. Finally many optimisations will have to be implemented before moving to realistic systems consisting of hundreds of molecules or more. One of the most important of these is the parallelisation of the code in order to efficiently use multiple processors.

Appendix A

Derivations

A.1 Preservation of the Norm

A.1.1 Ehrenfest

The statement of the conservation of norm is:

$$\sum_{l}^{N_{states}} \frac{d}{dt} |C_l^{(I)}|^2 = 0$$

Using chain rule (and assuming this hold for each replica) we can write this as:

$$\sum_{l}^{N_{states}} \frac{d}{dt} |C_l|^2 = \left(\frac{d}{dt} C_l^*\right) C_l + C_l^* \left(\frac{d}{dt} C_l\right)$$

If we write, $C_l = (a + bi)$ and $C_l^* = (a - bi)$ we can see the following relation holds:

$$\sum_{l}^{N_{states}} \frac{d}{dt} |C_l|^2 = \sum_{l}^{N_{states}} \left(\frac{d}{dt} C_l^*\right) C_l + C_l^* \left(\frac{d}{dt} C_l\right) = \sum_{l}^{N_{states}} 2\mathscr{R}\left[C_l^* \left(\frac{d}{dt} C_l\right)\right]$$

We have an expression for the time-derivative of the adiabatic expansion coefficient, under Ehrenfest (equation (??)). Inserting this above we get:

$$\sum_{l}^{N_{states}} \frac{d}{dt} |C_l|^2 = \sum_{l}^{N_{states}} 2\mathscr{R}\left[C_l^* \frac{-i}{\hbar} C_l \varepsilon_l - \sum_{k} C_l^* C_k d_{lk}^{ad}\right]$$

The first term is imaginary so we can remove it, as we're only interested in the real components:

$$\sum_l^{N_{states}} \frac{d}{dt}|C_l|^2 = -2\sum_{l,k}^{N_{states}} \mathscr{R}\left[C_l^* C_k d_{lk}^{ad}\right]$$

The next term is exactly zero due to the anti-symmetry of the NACE that is the equation above can be written as:

$$\sum_l^{N_{states}} \frac{d}{dt}|C_l|^2 = -2\sum_{k=2}^{N_{states}} \sum_{l<k} \mathscr{R}\left[(C_l^* C_k - C_k^* C_l)d_{lk}\right] = 0$$

A.1.2 CTMQC

The proof of conservation of the norm in CTMQC is similar to Ehrnfest. Again we write:

$$\sum_l^{N_{states}} \frac{d}{dt}|C_l|^2 = \sum_l^{N_{states}} 2\mathscr{R}\left[C_l^*\left(\frac{d}{dt}C_l\right)\right]$$

This time, the propagtion equation is slightly different:

$$\sum_l^{N_{states}} \frac{d}{dt}|C_l|^2 = \sum_l^{N_{states}} 2\mathscr{R}\left[C_l^* \frac{-i}{\hbar}C_l\varepsilon_l - \sum_k C_l^* C_k d_{lk}^{ad} - \sum_{\nu=1}^{N_n}\sum_k \frac{\mathscr{Q}_{lk,\nu}^{(I)}}{\hbar M_\nu}\cdot\left(\mathbf{f}_{k,\nu}^{(I)} - \mathbf{f}_{l,\nu}^{(I)}\right)|C_k|^2 C_l^{(I)} C_l^{*\ (I)}\right]$$

We have seen that the Ehrenfest part of the above equation conserves the norm, so we can remove that. we can also combine the $2\ C_l$ terms on the end:

$$\sum_l^{N_{states}} \frac{d}{dt}|C_l|^2 = -2\sum_{l,k}^{N_{states}} \mathscr{R}\left[\sum_{\nu=1}^{N_n} \frac{\mathscr{Q}_{lk,\nu}^{(I)}}{\hbar M_\nu}\cdot\left(\mathbf{f}_{k,\nu}^{(I)} - \mathbf{f}_{l,\nu}^{(I)}\right)|C_k|^2|C_l^{(I)}|^2\right]$$

Because $\mathscr{Q}_{lk,\nu}^{(I)} = \mathscr{Q}_{kl,\nu}^{(I)}$ (and the diagonal is undefined) we can re-write the above equation as:

$$\sum_l^{N_{states}} \frac{d}{dt}|C_l|^2 = -2\sum_l^{N_{states}} \sum_{k<l} \mathscr{R}\left[\sum_{\nu=1}^{N_n} \frac{\mathscr{Q}_{lk,\nu}^{(I)}}{\hbar M_\nu}\cdot\left[\left(\mathbf{f}_{k,\nu}^{(I)} - \mathbf{f}_{l,\nu}^{(I)}\right) + \left(\mathbf{f}_{l,\nu}^{(I)} - \mathbf{f}_{k,\nu}^{(I)}\right)\right]|C_k|^2|C_l^{(I)}|^2\right] = 0$$

So the norm should be conserved for each replica in CTMQC.

A.2 Rabi Oscillation

By only allowing one parameter to vary in the propagation one can isolate and test that. For the electronic propagation I held the nuclear positions constant resulting in rabi oscillation. This is due to the Schrödinger equation changing from a partial differential equation to, an analytically solvable, ordinary differential equation i.e:

$$\hbar \frac{\delta}{\delta t} \Phi(\mathbf{R}(t),t) = \hat{H}(\mathbf{R}(t),t)\Phi(\mathbf{R}(t),t)$$

$$\downarrow$$

$$\hbar \frac{d}{dt} \Phi(t) = \hat{H}(t)\Phi(t)$$

Which has the general solution:

$$\Phi(t) = e^{\hbar \hat{H} t}\Phi(0)$$

Appendix B

FOB Formalism

The effect of the nuclei on the electrons is normally handled via the Hamiltonian. This is dependent on nuclear positions and is in turn used in the Schrödinger equation to propagate the electron dynamics. Often the construction of the Hamiltonian is carried out using density function theory (DFT). However, for large, dynamic systems this becomes too computationally expensive and a different technique should be used. In this work I will rely on an Analytical Overlap Method (AOM)[50] to calculate the off-diagonal elements of the Hamiltonian. The diagonal elements will be calculated via a forcefield.

B.1 AOM

AOM assumes that the off-diagonal elements of the Hamiltonian are proportional to the off-diagonal elements of the overlap matrix between 2 singly occupied molecular orbitals (SOMO) see figure B.1. This is show in equation (B.1).

$$H_{kl} = CS_{kl} \qquad \text{(B.1)}$$

This approximation was originally by Longuet-Higgins and Roberts[51] and its validity has been tested in our group previously in the small overlap regime[50]. Many of the presently most studied and promising organic semiconductors, such as Rubrene[52,53] and Pentacene[54,55] have pi-conjugation. In these systems
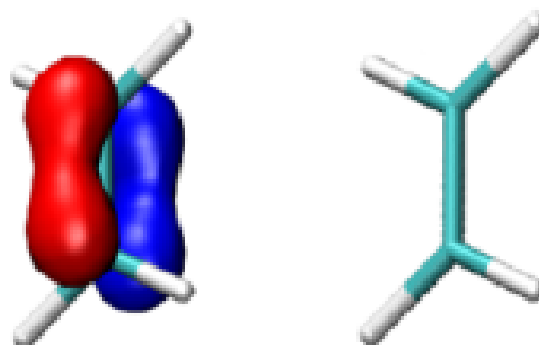
Figure B.1: A depiction of a singly occupied molecular orbital (SOMO) on an ethylene molecule. Adapted from[44].

it is often sufficient to include only 1 optimised p-orbital per atom[44]. This gives us an equation for the overlap of the SOMOs (φ_k) as:

$$S'_{kl} = \langle \varphi_k | \varphi_l \rangle = \sum_{i \in k}^{atoms} \sum_{j \in l}^{atoms} c^*_{p\pi,i} c_{p\pi,j} \langle p_{\pi,i} | p_{\pi,j} \rangle \tag{B.2}$$

Where $\langle p_{\pi,i} |$ represents the optimised Slater p-orbital and the $c_{p\pi,i}$ terms are the AOM expansion coefficients. The gradient of the Hamiltonian can also be expressed in terms of the gradient of the overlap $\nabla_\nu H_{kl} = C \nabla_\nu S_{kl}$ (where ν represents the atom index). Further efficiencies can be made by expressing the gradient of the overlap in terms of (diabatic) NACVs e.g:

$$\nabla_\nu H'_{kl} = C \nabla_\nu S'_{kl} = C \nabla_\nu \langle \varphi_k | \varphi_l \rangle = C(\mathbf{d}'^*_{\nu,lk} + \mathbf{d}'_{\nu,kl}) \tag{B.3}$$

Where we have defined the non-adiabatic coupling vectors (in a non-orthogonal diabtic basis) as $\mathbf{d}'_{\nu,lk} = \langle \varphi_l | \nabla_\nu \varphi_k \rangle$. The H'_{kl} term is the Hamiltonian in the non-orthogonal diabatic basis. The NACVs are calculated via a finite difference method.

B.2 Different Bases

The definitions in the previous section giving the key points in the AOM method were all expressed in a non-orthogonal diabatic basis. However, the electronic propagation in the FOB method is done in an orthogonal diabatic basis denoted ϕ_l. Further the CTMQC equations have been derived and are expressed in the adiabtic basis, ψ_l. Therefore, it is important to define the transformations between the 3 bases used in the code.

B.2.0.1 Basis Expansion

The time-dependent electronic wavefunction can be expressed as a linear combination of basis functions with expansion coefficients determining the size of their contribution. For example:

$$\Phi_{\mathbf{R}}(\mathbf{r},t) = \sum_n^{N_{states}} C_n(\mathbf{R},t) \psi_{\mathbf{R},n}(\mathbf{r}) = \sum_l^{N_{states}} u_l(\mathbf{R},t) \phi_{\mathbf{R},l}(\mathbf{r}) \tag{B.4}$$

Where $\Phi_{\mathbf{R}}(\mathbf{r},t)$ is the electronic wavefunction in the exact factorisation formalism. The subscript $\mathbf{R}$ denotes a parametric dependence on nuclear coordinates, the subscript n denote adiabatic state n similarly l denotes the lth (orthogonal) diabatic state. Throughout this document I will use the

following naming convention: $\mathbf{R}$ denotes nuclear coordinates and $\mathbf{r}$ for the electronic coordinates. The C_l is the lth adiabatic state. The squared modulus of this gives the population of electrons on that state. Expressing the electronic wavefunction in this way allows us to rewrite the propagation equations in terms of the expansion coefficients C_l or u_l.

As the propagation equations are written in terms of the expansion coefficients it is sensible to give the transformation equation in terms of them. To transform from the adiabatic to diabatic basis we can use the following unitary transformation:

$$\vec{C}(\mathbf{R},t) = \mathbb{U}(\mathbf{R},t)\, \vec{u}(\mathbf{R},t) \tag{B.5}$$

Here we have expressed the expansion coefficients as a vector e.g. $\vec{C} = \begin{pmatrix} C_1 \\ \vdots \\ C_n \end{pmatrix}$ The unitary transformation matrix is given as the overlap between diabatic and adiabatic states, $U_{ln} = \langle \phi_l | \psi_n \rangle$, and is a square matrix of size N_{states}^2. This is obtained by diagonalising the Hamiltonian in the code. The fact that this matrix is unitary means transforming from the diabatic to adiabatic is no more computationally expensive. The transformation can be obtained by pre-multiplying both sides of eq (B.5) by $\mathbb{U}^\dagger$ e.g.

$$\mathbb{U}^\dagger(\mathbf{R},t)\vec{C}(\mathbf{R},t) = \vec{u}(\mathbf{R},t) \tag{B.6}$$

To transform from the non-orthogonal to orthogonal basis we need a new matrix. This is given by:

$$\vec{\phi} = \mathbb{T}\vec{\varphi} \tag{B.7}$$

This transformation is needed when transforming the non-orthogonal diabatic Hamiltonian, H', and non-adiabatic coupling terms to the orthogonal diabatic basis. For example, the orthogonal diabatic Hamiltonian is calculated as $H_{kl} = \left[\mathbb{T}^{-1}\mathbb{H}'\mathbb{T} \right]_{kl}$. This matrix is equal to the inverse square of the overlap between SOMOs i.e. $T_{ml} = [\mathbb{S}^{-\frac{1}{2}}]_{ml}$.

Replacing the full charge transfer determinant with parametrised singly occupied molecular orbitals (SOMOs) makes the calculation of the relevant terms in the propagation of the system very efficient. The approximation has been scrutinised before in the group[44,50,56–59] and its first implementation within the surface hopping framework has been shown to reproduce known phenomena such as the crossover from band-like to hopping-like transport[56]. In this way the interaction of the nuclei on the electrons is accounted for, as the overlap between SOMOs (and therefore the coupling, H_{ab}) depends on the nuclear geometry.

Thankfully, previous members of the group (see Spencer et al[44]) have implemented the FOB method within the surface hopping framework in CP2K -an ab-initio molecular dynamics package. I will therefore be able to reuse/adapt a large number of the subroutines in my implementation of the FOB-CTMQC method within CP2K.

Appendix C

Colophon

This document was set in the Time Roman typeface using LaTeXand BibTeX, composed with the Atom text editor. The Python programming language was used for all plots and data analysis. Our group's own flavour of the CP2K software package was used to produce all data.

Bibliography

[1] C. K. Chiang, C. R. Fincher, Y. W. Park, A. J. Heeger, H. Shirakawa, E. J. Louis, S. C. Gau, and Alan G. MacDiarmid. Electrical Conductivity in Doped Polyacetylene. *Physical Review Letters*, 39(17):1098–1101, October 1977.

[2] Hideki Shirakawa, Edwin J. Louis, Alan G. MacDiarmid, Chwan K. Chiang, and Alan J. Heeger. Synthesis of electrically conducting organic polymers: halogen derivatives of polyacetylene, (CH)x. *J. Chem. Soc., Chem. Commun.*, 0(16):578–580, Jan 1977.

[3] Bernard Kippelen and Jean-Luc Brédas. Organic photovoltaics. *Energy Environ. Sci.*, 2(3):251–261, 2009.

[4] M. J. Małachowski and J. Żmija. Organic field-effect transistors. *Opto-Electron. Rev.*, 18(2):121–136, Jun 2010.

[5] N. Thejo Kalyani and S. J. Dhoble. Organic light emitting diodes: Energy saving lighting technology—A review. *Renewable Sustainable Energy Rev.*, 16(5):2696–2723, Jun 2012.

[6] OLED Display Market Tracker - Q2 2018 - IHS Technology, Nov 2018. [Online; accessed 23. Nov. 2018].

[7] Sebastian Reineke, Frank Lindner, Gregor Schwartz, Nico Seidler, Karsten Walzer, Björn Lüssem, and Karl Leo. White organic light-emitting diodes with fluorescent tube efficiency. *Nature*, 459(7244):234, May 2009.

[8] Kazuki Kato, Toshihiko Iwasaki, and Takatoshi Tsujimura. Over 130 lm/w all-phosphorescent white oleds for next-generation lighting. *Journal of Photopolymer Science and Technology*, 28:335–340, 10 2015.

[9] J. S. Brown and S. E. Shaheen. Introducing correlations into carrier transport simulations of disordered materials through seeded nucleation: impact on density of states, carrier mobility, and carrier statistics. *J. Phys.: Condens. Matter*, 30(13):135702, Mar 2018.

[10] I. Yavuz. Dichotomy between the band and hopping transport in organic crystals: insights from experiments. *Physical Chemistry Chemical Physics*, 19(38):25819–25828, 2017.

[11] Harald Oberhofer, Karsten Reuter, and Jochen Blumberger. Charge Transport in Molecular Materials: An Assessment of Computational Methods. *Chem. Rev.*, 117(15):10319–10357, August 2017.

[12] John C. Tully. Nonadiabatic Dynamics. pages 34–71.

[13] Simone Pisana, Michele Lazzeri, Cinzia Casiraghi, Kostya S. Novoselov, A. K. Geim, Andrea C. Ferrari, and Francesco Mauri. Breakdown of the adiabatic Born–Oppenheimer approximation in graphene. *Nat. Mater.*, 6(3):198, Feb 2007.

[14] M. Born and R. Oppenheimer. Zur Quantentheorie der Molekeln. *Ann. Phys.*, 389(20):457–484, Jan 1927.

[15] Sharon Hammes-Schiffer. Theoretical Perspectives on Proton-Coupled Electron Transfer Reactions. *Acc. Chem. Res.*, 34(4):273–281, Apr 2001.

[16] Sharon Hammes-Schiffer and John C. Tully. Proton transfer in solution: Molecular dynamics with quantum transitions. *J. Chem. Phys.*, 101(6):4657–4667, Sep 1994.

[17] John C. Tully. Nonadiabatic molecular dynamics. *International Journal of Quantum Chemistry*, 40(S25):299–309, 1991.

[18] Raymond Kapral and Giovanni Ciccotti. Mixed quantum-classical dynamics. *J. Chem. Phys.*, 110(18):8919–8929, May 1999.

[19] Todd J. Martínez∗. Insights for Light-Driven Molecular Devices from Ab Initio Multiple Spawning Excited-State Dynamics of Organic and Biological Chromophores. *American Chemical Society*, Oct 2005.

[20] Guillermo Albareda, Heiko Appel, Ignacio Franco, Ali Abedi, and Angel Rubio. Correlated Electron-Nuclear Dynamics with Conditional Wave Functions. *Phys. Rev. Lett.*, 113(8):083003, Aug 2014.

[21] John C. Tully. Molecular dynamics with electronic transitions. *J. Chem. Phys.*, 93(2):1061–1071, Jul 1990.

[22] R. L et al Whetten. Molecular dynamics beyond the adiabatic approximation: New experiments and theory. *Ann. Rev. Phys. Chem.*, 36:277–320.

[23] Neil Shenvi, Joseph E. Subotnik, and Weitao Yang. Simultaneous-trajectory surface hopping: A parameter-free algorithm for implementing decoherence in nonadiabatic dynamics. *J. Chem. Phys.*, 134(14):144102, Apr 2011.

[24] D. F. Coker and L. Xiao. Methods for molecular dynamics with nonadiabatic transitions. *J. Chem. Phys.*, 102(1):496–510, Jan 1995.

[25] Xiaosong Li, John C. Tully, H. Bernhard Schlegel, and Michael J. Frisch. Ab initio Ehrenfest dynamics. *J. Chem. Phys.*, 123(8):084106, Aug 2005.

[26] Kenichiro Saita and Dmitrii V. Shalashilin. On-the-fly ab initio molecular dynamics with multi-configurational Ehrenfest method. *J. Chem. Phys.*, 137(22):22A506, Dec 2012.

[27] Daniela Kohen, Frank H. Stillinger, and John C. Tully. Model studies of nonadiabatic dynamics. *J. Chem. Phys.*, 109(12):4713–4725, Sep 1998.

[28] John C. Tully. Perspective: Nonadiabatic dynamics theory. *The Journal of Chemical Physics*, 137(22):22A301, December 2012.

[29] Priya V. Parandekar and John C. Tully. Detailed Balance in Ehrenfest Mixed Quantum-Classical Dynamics. *Journal of Chemical Theory and Computation*, 2(2):229–235, March 2006.

[30] Federica Agostini, Seung Kyu Min, Ali Abedi, and E. K. U. Gross. Quantum-Classical Nonadiabatic Dynamics: Coupled- vs Independent-Trajectory Methods. *Journal of Chemical Theory and Computation*, 12(5):2127–2143, May 2016.

[31] Ali Abedi, Neepa T. Maitra, and E. K. U. Gross. Exact Factorization of the Time-Dependent Electron-Nuclear Wave Function. *Physical Review Letters*, 105(12), September 2010.

[32] Ali Abedi, Federica Agostini, Yasumitsu Suzuki, and E. K. U. Gross. Dynamical Steps that Bridge Piecewise Adiabatic Shapes in the Exact Time-Dependent Potential Energy Surface. *Physical Review Letters*, 110(26), June 2013.

[33] Graeme H. Gossel, Federica Agostini, and Neepa T. Maitra. Coupled-Trajectory Mixed Quantum-Classical Algorithm: A Deconstruction. *Journal of Chemical Theory and Computation*, August 2018.

[34] Federica Agostini, Ali Abedi, Yasumitsu Suzuki, Seung Kyu Min, Neepa T. Maitra, and E. K. U. Gross. The exact forces on classical nuclei in non-adiabatic charge transfer. *The Journal of Chemical Physics*, 142(8):084303, February 2015.

[35] Federica Agostini, Seung Kyu Min, and E. K. U. Gross. Semiclassical analysis of the electron-nuclear coupling in electronic non-adiabatic processes. *Annalen der Physik*, 527(9-10):546–555, October 2015.

[36] Federica Agostini, Ali Abedi, Yasumitsu Suzuki, and E.K.U. Gross. Mixed quantum-classical dynamics on the exact time-dependent potential energy surface: a fresh look at non-adiabatic processes. *Molecular Physics*, 111(22-23):3625–3640, December 2013.

[37] Seung Kyu Min, Ali Abedi, Kwang S. Kim, and E. K. U. Gross. Is the Molecular Berry Phase an Artifact of the Born-Oppenheimer Approximation? *Phys. Rev. Lett.*, 113(26):263004, Dec 2014.

[38] Farnaz A. Shakib and Pengfei Huo. Ring Polymer Surface Hopping: Incorporating Nuclear Quantum Effects into Nonadiabatic Molecular Dynamics Simulations. *J. Phys. Chem. Lett.*, 8(13):3073–3080, Jul 2017.

[39] Basile F. E. Curchod, Ivano Tavernelli, and Ursula Rothlisberger. Trajectory-based solution of the nonadiabatic quantum dynamics equations: an on-the-fly approach for molecular dynamics simulations, Feb 2011.

[40] Ivano Tavernelli. Ab initio–driven trajectory-based nuclear quantum dynamics in phase space. *Phys. Rev. A*, 87(4):042501, Apr 2013.

[41] Arne Scherrer, Federica Agostini, Daniel Sebastiani, E. K. U. Gross, and Rodolphe Vuilleumier. Nuclear velocity perturbation theory for vibrational circular dichroism: An approach based on the exact factorization of the electron-nuclear wave function. *J. Chem. Phys.*, 143(7):074106, Aug 2015.

[42] J. VandeVondele, J; Hutter. Gaussian basis sets for accurate calculations on molecular systems in gas and condensed phases. *The Journal of Chemical Physics*, 127(11).

[43] Seung Kyu Min, Federica Agostini, Ivano Tavernelli, and E. K. U. Gross. Ab Initio Nonadiabatic Dynamics with Coupled Trajectories: A Rigorous Approach to Quantum (De)Coherence. *The Journal of Physical Chemistry Letters*, 8(13):3048–3055, July 2017.

[44] J. Spencer, F. Gajdos, and J. Blumberger. FOB-SH: Fragment orbital-based surface hopping for charge carrier transport in organic and biological molecules and materials. *The Journal of Chemical Physics*, 145(6):064102, August 2016.

[45] John C. Tully. Nonadiabatic Dynamics. pages 34–71, 1998.

[46] John E. Anthony. The Larger Acenes: Versatile Organic Semiconductors. *Angew. Chem. Int. Ed.*, 47(3):452–483, Jan 2008.

[47] C. D. Dimitrakopoulos and D. J. Mascaro. Organic thin-film transistors: A review of recent advances. *IBM J. Res. Dev.*, 45(1):11–27, Jan 2001.

[48] Hisahiro Sasabe and Junji Kido. Multifunctional Materials in High-Performance OLEDs: Challenges for Solid-State Lighting. *Chem. Mater.*, 23(3):621–630, Feb 2011.

[49] Chr. Cattarius, G. A. Worth, H.-D. Meyer, and L. S. Cederbaum. All mode dynamics at the conical intersection of an octa-atomic molecule: Multi-configuration time-dependent Hartree (MCTDH) investigation on the butatriene cation. *The Journal of Chemical Physics*, 115(5):2088–2100, August 2001.

[50] Fruzsina Gajdos, Siim Valner, Felix Hoffmann, Jacob Spencer, Marian Breuer, Adam Kubas, Michel Dupuis, and Jochen Blumberger. Ultrafast Estimation of Electronic Couplings for Electron Transfer between pi-Conjugated Organic Molecules. *Journal of Chemical Theory and Computation*, 10(10):4653–4660, October 2014.

[51] Oleg V. Prezhdo and Peter J. Rossky. Evaluation of quantum transition rates from quantum-classical molecular dynamics simulations. *J. Chem. Phys.*, 107(15):5863–5878, Oct 1997.

[52] Daniele Braga and Gilles Horowitz. High-Performance Organic Field-Effect Transistors. *Adv. Mater.*, 21(14-15):1473–1486, Feb 2009.

[53] Behzad Barış, Hatice Gürel Özdemir, Nihat Tuğluoğlu, Serdar Karadeniz, Ömer Faruk Yüksel, and Zeynep Kişnişci. Optical dispersion and dielectric properties of rubrene organic semiconductor thin film. *J. Mater. Sci. - Mater. Electron.*, 25(8):3586–3593, Aug 2014.

[54] Shree Prakash Tiwari, William J. Potscavage, Tissa Sajoto, Stephen Barlow, Seth R. Marder, and Bernard Kippelen. Pentacene organic field-effect transistors with doped electrode-semiconductor contacts. *Org. Electron.*, 11(5):860–863, May 2010.

[55] Tae-Young Kim, Jingon Jang, Kyungjune Cho, Younggul Song, Woanseo Park, Jinsu Park, Jae-Keun Kim, Woong-Ki Hong, and Takhee Lee. Interface effect in pentacene field-effect transistors from high energy proton beam irradiation. *Org. Electron.*, 27:240–246, Dec 2015.

[56] Samuele Giannini, Antoine Carof, and Jochen Blumberger. Crossover from Hopping to Band-Like Charge Transport in an Organic Semiconductor Model: Atomistic Nonadiabatic Molecular Dynamics Simulation. *The Journal of Physical Chemistry Letters*, 9(11):3116–3123, June 2018.

[57] Antoine Carof, Samuele Giannini, and Jochen Blumberger. Detailed balance, internal consistency, and energy conservation in fragment orbital-based surface hopping. *The Journal of Chemical Physics*, 147(21):214113, December 2017.

[58] Fruzsina Gajdos, Harald Oberhofer, Michel Dupuis, and Jochen Blumberger. On the Inapplicability of Electron-Hopping Models for the Organic Semiconductor Phenyl-C61-butyric Acid Methyl Ester (PCBM). *J. Phys. Chem. Lett.*, 4(6):1012–1017, Mar 2013.

[59] Jacob Spencer, Laura Scalfi, Antoine Carof, and Jochen Blumberger. Confronting surface hopping molecular dynamics with Marcus theory for a molecular donoracceptor system. *Faraday Discussions*, 195:215–236, 2016.